The International Journal of Advanced Manufacturing Technology
https://doi.org/10.1007/s00170-021-06873-2

ORIGINAL ARTICLE

Diagnostic and severity analysis of combined failures composed by imbalance and misalignment in rotating machines

Dionísio Henrique Carvalho de Sá Só Martins[1] · Denys Pestana Viana[1] · Amaro Azevedo de Lima[1] · Milena Faria Pinto[1] · Luís Tarrataca[1] · Fabrício Lopes e Silva[1] · Ricardo Homero Ramírez Gutiérrez[2] · Thiago de Moura Prego[1] · Ulisses Admar Barbosa Vicente Monteiro[2] · Diego Barreto Haddad[1]

Received: 11 December 2020 / Accepted: 5 March 2021

Abstract

Failure detection from mechanical vibration analysis is crucial in industry machinery, with early discovery allowing for preventive action to be performed. This paper introduces a prototype of an IoT system capable of (i) identifying combined failures of a rotating machine and (ii) predicting failures, in a non-invasive manner. An embedded solution is devised, which is able to classify four types of operating conditions, namely (i) normal, (ii) imbalanced, (iii) imbalanced associated with horizontal misalignment, and (iv) imbalanced associated with vertical misalignment. The goal of the paper is to propose an automatic method of diagnosis and measurement of combined failures in rotating machines. The employed methodology combines a simulation bench and measuring the severity in a controlled environment. Three distinct machine learning techniques were compared for classification purposes: support vector machines, *k*-nearest neighbors, and random forests. The results obtained reveal the possibility of differentiating between the types of combined faults; an accuracy of 81.41% using a random forest classifier was achieved. A supervisory system was developed which is responsible for monitoring machines and sending wireless alert messages. The latter are sent to a control application, allowing for user interaction through mobile devices. Results reveal the possibility of differentiating between the types of combined faults, and also motor failure severity profile for different scenarios. Through the construction of severity profiles, when faults occurred, high vibration values were registered at elevated speeds. The proposed methodology can be used in any rotating machine that complies with the conditions imposed by ISO 10816.

Keywords Machine failure prediction · Machinery combined faults diagnosis · Supervisory system

1 Introduction

The 4th industrial revolution is driven by a new productive paradigm that optimizes the execution of business models [1]. Due to the fact that rotating machinery are widely employed in modern industry, their fault diagnosis has also been a hot topic [2]. Rotating machines usually operate under a range of conditions, such as frequent load changes and high speeds. As a result, they are subject to performance degradation as well as mechanical failures [3]. Accurate and fast fault diagnosis is critical in industry in order to enhance system effectiveness and reliability [4, 5], which results in operation safety increases and maintenance cost reductions. The latter are of great importance for industries, where significant efforts to reduce these are made while maintaining product quality capable of sustaining competitiveness. Accordingly, it is important to optimize resources, plan for maintenance activities, comply with safety standards, and invest in ongoing research to develop and integrate maintenance tools [6]. As stated in [6], effective monitoring systems minimize unexpected failures and reduce service costs and unscheduled downtime. Over the past few decades, a variety of sensors have been employed to measure dynamic responses [7]. These can be used to monitor the equipment condition, such as mechanical vibration, temperature, electric current, and magnetic field [6]. Because of

✉ Dionísio Henrique Carvalho de Sá Só Martins
dionisiohenrique@ig.com.br

Denys Pestana Viana
denys.pestana@gmail.com

[1] Federal Center for Technological Education of Rio de Janeiro, Rio de Janeiro, Brazil

[2] Federal University of Rio de Janeiro, Brazil, Rio de Janeiro, Brazil

Published online: 21 April 2021

this, there is a growing interest in intelligent fault diagnosis methods capable of estimating machine conditions with high accuracy, such as the ones described in [8–10].

The useful life of a component at various degradation levels can be estimated by vibration signal analysis, as shown in [11] and [12]. Different types of faults can be identified by analyzing vibration signals. These can be detected through measurements made using sensors coupled with data acquisition systems. Such an approach allows for accurate results while also being non-invasive in nature. A non-invasive measurement method is one that does not require a part to be disassembled or removed from its position on the machine to check if it has any defects [13]. By employing a fault diagnosis system based on vibration analysis, electric motor operators are able to reduce or even prevent unexpected failures [14]. Failure detection from mechanical vibration analysis is crucial, since it allows for the detection of failures in bearings and gears at an early stage. This feature is of critical importance because it enables appropriate maintenance measures to be taken. When assessing the running operational condition of an electrical motor, the following measures are used to quantify the level of vibration: acceleration, velocity, or displacement [15].

1.1 Related work

Prognosis of rotating machines based on statistical methods and artificial intelligence has been the object of several papers in the recent years [16–21]. Such techniques are motivated by the fact that unexpected machinery failures are capable of causing significant losses in terms of time and production [22]. Rotating machines are susceptible to failures that, depending on the severity, can (i) cause unexpected production stoppages, (ii) put at risk operational personnel, (iii) produce negative environmental impacts, and (iv) lead to economic losses. According to [23], the most frequent failures are imbalance, misalignment, bent shaft, eccentricity, looseness, belt drive problems, gear defects, bearing defects, electrical faults, oil whip/whirl, hydraulic and aerodynamic forces, cavitation, shaft cracks, rotor rubs, and resonance. Of these, imbalance and misalignment, which are responsible for approximately 40% of failures in electric motors, are the most common failures during the useful life of rotating machines [23–25].

According to [26], misalignment is caused by improper installation, lack of symmetry in applied loads, and large in-site thermal variation. This problem induces several types of complications, such as early wear of mechanical couplings and bearings. Besides, misalignment can reduce machine efficiency [27]. Vibration analysis is one of the most powerful and reliable methods for determining misalignment during machine operation. The operating condition of electric motors can be evaluated by monitoring temperature, electric current, acoustic signals, and mechanical vibrations [28]. A rotor is considered imbalanced when its center of mass is out of alignment with its center of rotation. This may be due to the manufacturing process, assembly, wear, among others [29].

By analyzing the vibration spectrum, it is possible to detect misalignment as well as identify imbalance faults. Misalignment mainly occurs when the rotor is inadequately assembled in relation to the couplings and bearings. This fault can be identified when the vibration amplitude, in the axial direction, at fundamental frequency and at the first harmonic is high in relation to the other harmonics (i.e., angular misalignment) and at first harmonic in the radial direction (i.e., parallel misalignment). On the other hand, imbalance is a result of when the amplitude at the fundamental frequency of the machine working frequency is much higher than the amplitudes of the other harmonics in the radial direction.

Different methodologies have been proposed for failure diagnostics. In [6], the authors explained maintenance techniques based on the supervisory control and data acquisition (SCADA) system for monitoring electric motors in ships, since in this situation abrupt or unforeseen failures can cause great damage. They devised both non-invasive diagnostic and monitoring techniques that monitor the operational state of the motor. This strategy allows for the identification of significant increases of a given parameter with the objective of avoiding accidents. Reference [30] analyzed static imbalance faults by analyzing vibrations in a motor running at a constant frequency of 28.5 Hz. The paper advanced an intelligent algorithm in a field-programmable gate array (FPGA) device intending to correct imbalance defects. The proposed solution identified the type of failure and an appropriate corrective action.

In [31], a method based on ISO 10816 was proposed whose main objective of the paper was to establish a failure threshold for the equipment. This limit was based on the level of vibration emitted by the machine with fails at the rolling element bearing. Reference [32] analyzed several statistical measures associated with machine learning techniques in order to obtain the degree of fault severity in a rotating machine bearing. The analysis focused in the time and frequency domains. However, high levels of vibration were found to occur when there are defects in the inner and outer races of the bearing housing. Supervised classification algorithms were used to identify the type of defects. The fault severity profile was raised based on statistical measures such as kurtosis, entropy, RMS value of the acceleration signal, and crest factor. However, only isolated failures were evaluated and combined failures were not investigated.

In [33], a hybrid approach was proposed for the identification and measurement of the severity of isolated

faults inserted in a simulation bench made up of a three-phase electric induction motor. The approach combines the measurement of vibration signals and electrical signals. A triaxial accelerometer, a current sensor, and a voltage sensor were employed as sensors. The types of failures analyzed were imbalance, misalignment, rotor failure, and stator failure. In the first stage of the proposed approach, the vibration signals measured by the accelerometers were processed, using the ISO 10816 standard as a severity metric. In the second stage, the current and voltage signals were analyzed. The results show that the hybrid method outperforms those relying only on electrical parameters.

Work [34] aimed to measure and identify two types of misalignment in rotating machines, namely, parallel and angular. The following pre-processing steps were performed: normalization of the vibration signal, discrete wavelet transformation, and feature selection. Digital signal processing methods, artificial neural network classifiers, and support vector machine were used in order to diagnose the type of misalignment and to measure the severity level. Two different data sets were considered that were the result of (i) keeping the motor speed constant and varying the amount of misalignment, and (ii) varying the motor speed and keeping the amount of misalignment constant. The severity measurement parameter used in this article was the overall vibration level obtained from the acceleration signal. Severity profile curves were raised, varying the rotation speed and amount of misalignment of the rotating machine. The article proposes as future work the application of this method for the evaluation of combined faults of misalignment with imbalance.

In order to improve data analysis and signal processing techniques, it is important to understand machine, and component, operation. Both of which can be used to monitor equipment state. There are still improvements to be made in the area of equipment condition monitoring, as many of the analyses performed depend heavily on domain-specific knowledge [28]. More recently, signal processing techniques and intelligent algorithms have been proposed to estimate the underlying working state of rotating machines. Usually, signal processing-based fault detection for machines is performed in three stages, which are signal acquisition, feature extraction, and fault identification [35]. These strategies extract the features that reflect machine condition through time-domain analyses, frequency-domain analyses, or time-frequency analyses [36–38]. For fault classification, approaches based on meaningful features are extensively applied, such as artificial neural networks [39], support vector machines [40, 41], and fuzzy logic [42].

In recent years, research has been carried out to identify and measure combined failures in rotating machines. Methods have been proposed based on mathematical models of the simulation benches mechanical systems [43, 44] or artificial intelligence [45]. However, as far as the authors' knowledge is concerned, up to the present time, no study of the severity profile for combined failures has been proposed yet, making this article an innovate work.

1.2 Main contributions

From the previous literature review, it is possible to perceive that few studies investigate the diagnosis of *combined* faults in rotating machines. Additionally, most research focuses on the diagnosis of single faults, i.e., they aim to identify only one type of failure at a time. In contrast, this paper focuses on diagnosing and measuring combined faults, composed of imbalance associated with misalignment in rotating machines, using machine learning algorithms. Namely, our main objectives consist in (i) providing reliable combined fault identification and prediction through severity estimation, and (ii) measure and compare the severity profile of combined imbalance faults alongside misalignment faults in relation to simple imbalance faults.

The novelty of this paper is the application of experimental techniques capable of identifying the combined failures in rotating machines and measuring its severity. The method proposed in this article can be widely used in applications in industrial machines to condition-based maintenance for mining machines, electric motors, manufacturing tools, and wind turbines. This technique can be used for manufacturing in marine oil and gas industrial segments. The proposed methodology can be used in any rotating machine that complies with the conditions imposed by ISO 10816.

1.3 Organization

The remainder of this work is organized as follows: Section 2 details the proposed methodology for severity analysis on machines and its foundations; Section 3 presents the proposed supervisory system and its main functionalities; Section 4 describes the experiments performed and discusses the results; and Section 5 presents the concluding remarks.

2 Imbalance severity analysis methodology on rotating machines

One of the main objectives of this paper is to evaluate a failure diagnosis system and its ability to determine the respective severity degree. Therefore, an experimental bench and a data acquisition system were constructed. In this work, the experimental bench Alignment Balance Vibration Trainer (ABVT), presented in Fig. 1, was used to simulate failure and the corresponding severity. The system is composed of a DC motor with approximately

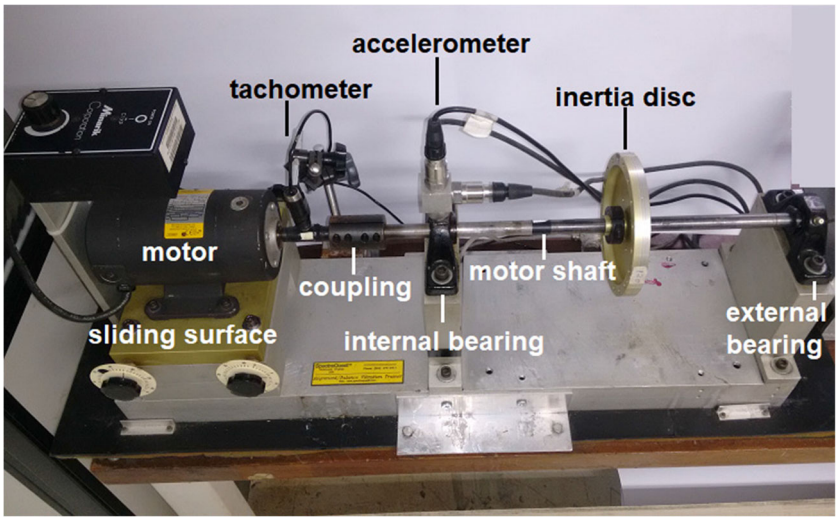

Fig. 1 Experimental bench ABVT

184 W of power, a thin shaft, bearings, and an inertia disc with roles to add masses. This system was employed to study different scenarios in a parametric way, namely, we focused on normal behavior, imbalanced rotor, horizontal misalignment, and vertical misalignment.

The imbalance defect is inserted into the workbench by placing screws with a known mass on the inertia disc. The horizontal misalignment defect is produced by moving the base of the DC motor in the horizontal direction and measuring its position with a digital caliper. Vertical misalignment results from the addition of known thickness shims at the base of the electric motor. In order to train and evaluate the advanced methods, 353 split signals were recorded, as described in Table 1. The imbalance values correspond to the value of the masses in grams that were inserted in the inertia disc, while the values of misalignments in millimeters refer to the displacement of the motor base in relation to its original position. As will later be shown in Section 4.1, tests comparing the use of piezoelectric and capacitive sensors showed the latter were only able to record in an adequate manner normal signals, while the former presented better results. Consequently, the piezoelectric accelerometer was chosen to analyze failure signals. For the vibration signal acquisition, through piezoelectric and capacitive sensors, we employed a dynamic signal acquisition module (NI 9234), manufactured by National Instruments. A tachometer was used in the DC motor to monitor its speed. The signal was acquired with the aid of a LabView application and the signal processing was carried out using MATLAB. An Arduino Uno was used to send the failure information presented on the experimental bench and its severity to a cell phone. The remainder of this section is organized as follows: Section 2.1 describes the accelerometer types used in the experiments, and Section 2.2 briefly describes the criteria for severity measurement.

2.1 Accelerometers types

The vibration signals of the internal bearing, as presented in Fig. 1, were measured using piezoelectric and capacitive accelerometers. In addition, a tachometer was used to obtain motor speed. The piezoelectric accelerometer has the following characteristics: frequency range $f \in [0.27, 10000]$ Hz, acceleration measurement range $f \in [-50g, 50g]$, and sensitivity 100 mV/g ($\pm 20\%$). Three

Table 1 Different scenarios employed for testing

Scenarios	Number of signals	
	Piezoelectric	Capacitive
Normal	115	115
Imbalance (6g)	23	0
Imbalance (20g)	18	0
Imbalance (6g) + horizontal misalignment (1 mm)	23	0
Imbalance (20g) + horizontal misalignment (1 mm)	18	0
Imbalance (6g) + vertical misalignment (1.27 mm)	23	0
Imbalance (20g) + vertical misalignment (1.27 mm)	18	0

uniaxial accelerometers of this type were used to measure acceleration in directions perpendicular to each other (X, Y, and Z directions).

The operating principle of this sensor is based on the piezoelectric effect inherent to the built-in crystal. The piezoelectric crystal generates a voltage signal proportional to the mechanical stress intensity. Conversely, when subjected to a voltage difference, the material vibrates. This happens because there is a change in the crystalline structure of the material when an effort is applied to the material. The atoms change position, thus causing a change in the electrical polarity of the material [46].

Piezoelectric accelerometers have several advantages, namely their linearity (in its working frequency range) and they are simple to manufacture when compared to capacitive accelerometers. On the other hand, they present inadequate DC response due to the leakage phenomenon that occurs in piezoelectric materials. Furthermore, this type of sensor also requires large casings [47]. The capacitive accelerometer used features a measurement frequency $f \in [10, 20000]$ (Hz), acceleration measurement amplitude range of $[-50$ to $50]$ g, and 1000 mV/g ($\pm 10\%$) sensitivity. A triaxial accelerometer was chosen so that measurement accelerations could be performed in the X, Y, and Z directions.

A capacitive accelerometer is essentially composed of a fixed plate that is attached to the component housing and a movable plate that contains the inertial mass. These plates are positioned in parallel at a distance d. This distance varies as the body vibrates, which translates into a capacitance change. The difference also affects the output of the electrical signal emitted by the sensor, corresponding to an acceleration variation [48]. Capacitive accelerometers have low cost, thermal stability, and produce low noise. However, they are sensible to electromagnetic interference and have low accuracy when compared to industrial piezoelectric accelerometers [47].

In order to choose which of the accelerometers would be used, experiments were carried out where the signals were recorded by varying the motor speed in the range $f \in [16, 60]$ (Hz) range (with steps of 2 Hz). The results of these experiments are presented in Section 4.1. The process resulted in 23 signals distinct from normal system operation. This procedure was then repeated five times for each accelerometer, totaling 115 signals, and allowed us to verify the sensors precision.

2.2 Severity measurement criteria

ISO 10816 [49] is the international standard that defines the procedures classifying severities on rotating machines. The standard imposes certain requirements in order to assess the state of a machine from vibration signals, e.g., restricting signal bandwidth, proper sensor mounting location, motor operating speed, ambient temperature, ambient vibration level, and system resonance frequencies. The standard also describes ways of measuring the severity of the vibration signals. Our work uses the vibration default value described in the standard as the vibration value that corresponds to the severity profile of the machine in its normal operating condition.

3 Proposed supervisory system

We chose to develop a supervisory system responsible for (i) identifying motor failure occurrence, (ii) assessing the corresponding defect level, (iii) sending alert messages via Bluetooth to a mobile device, and (iv) turning off the motor automatically in case of a critical fault.

It is important to emphasize that the vibration signal needs to be preprocessed, before any feature extraction signal can be performed. This is due to the high noise level that is present in the signal acquired directly from the sensors. When the noise impact is not properly addressed, significant changes occur in the acceleration signal integration result, impairing the machine severity determination [50]. The signals were acquired via Labview and processed with MATLAB. The latter was used to perform signal filtering, signal integration, defect diagnosis, defect severity calculation, and the supervisory system user interface.

The block diagram of the supervisory system is depicted in Fig. 2 and the remainder of this section is organized to detail this structure, namely Section 3.1 briefly describes the filtering stage; Section 3.2 presents the integration and severity determination stages; Section 3.3 describes the feature extraction process; Fault Diagnosis is shown in the Section 3.3.1; interfacing with Arduino is described Sections 3.4; and 3.5 addresses the supervisory screen output.

3.1 Filtering

Signal filtering is one of the steps required to perform fault diagnosis and fault severity estimation based on vibration signals since they present a high level of noise that can misrepresent the information. At this stage, the utilized bandpass filter rejects frequencies that lie outside the range $10 - 1000$ Hz.

3.2 Integration and severity determination

ISO 10816 norm utilizes the mean square value of the velocity signal to calculate the severity measurement. As a result, after filtering the acceleration signal, an integration step is required to obtain the vibration velocity signal.

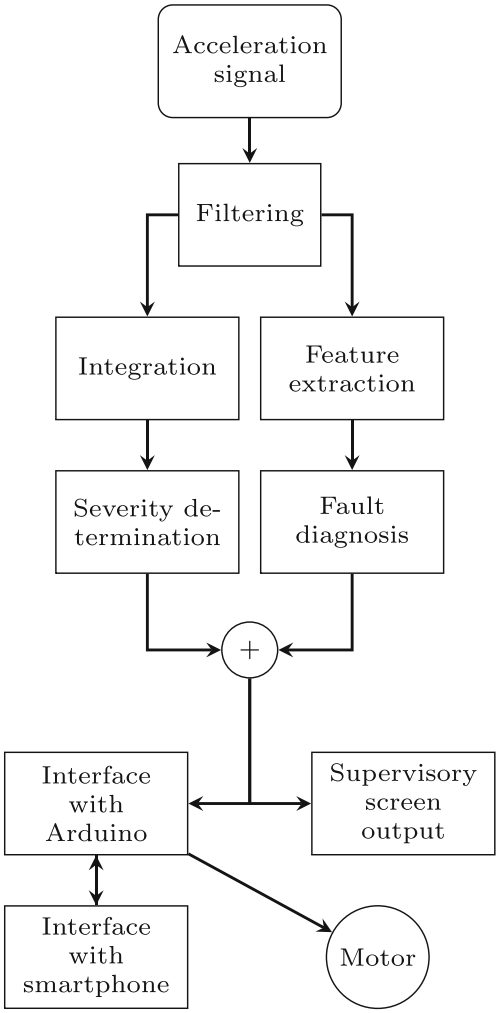

Fig. 2 Block diagram of the proposed supervisory system

Unfortunately, vibration signals are composed of several harmonic components and have a complex formation structure. Therefore, it is recommended to eliminate the direct current (DC) component of the signal before integrating the accelerometer signal [50]. It is impracticable to completely remove the DC component of the acceleration signal. Consequently, there is an offset value in the time-domain integration result [50].

To perform a frequency-domain integration, it is possible to measure the frequency of the acceleration signal through the fast Fourier transform algorithm. This efficiently evaluates the discrete time Fourier transformation. Subsequently, algebraic operations are performed in order to find the vibration frequency from the acceleration spectrum. These operations employ the inverse Fourier transformation to obtain the vibration speed signal in the time domain:

$$v(n) = \sum_{k=0}^{N-1} \frac{1}{j2\pi k \Delta_f} A(k) e^{j2\pi nk/N}, \quad (1)$$

where Δ_f denotes the frequency resolution, $j \triangleq \sqrt{-1}$, N is the window size, and $A(k)$ is the Fourier transform of the acceleration signal, whose integration is performed in the frequency domain.

Frequency domain integration is able to achieve acceleration signal integration effectively when the frequency components of the measured acceleration signal are relatively high [51]. This is also recommended for practical applications [52]. The operation requires the signal to be processed by a bandpass filter and that no spectral leakage occurs.

The severity is determined based on the root mean square (RMS) values of the vibration speed recorded under a normal condition operation. From these measurements, four severity ranges were established relating to motor condition (Table 2), based on the knowledge of the operation of this simulation bench. The algorithm first checks which of the three directions (X, Y, or Z) has the highest RMS value of vibration velocity (V_{RMS}). Then, V_{RMS} is compared with the normal operating condition reference value $V_r^{(\mathrm{dir})}$, where (dir) can be X, Y, or Z. Finally, the algorithm decides which severity range the signal belongs to.

The proposed methodology can be used in any rotating machine that complies with the conditions imposed by ISO 10816. However, it is necessary to take into consideration the rotation range from 2 to 250 Hz for rotating machines with electrical power up to 15 kW. The comparison measure can be made in a relative way by analyzing the normal functioning profile of the equipment under analysis and comparing it with the cases of failures that may occur [49].

3.3 Feature extraction and fault diagnosis

The feature extraction process that allows for discrimination between different failure types can be performed using time domain, frequency domain, or a combination of both techniques [11]. This procedure creates fault patterns for a particular defect, which in turn can be classified by machine learning algorithms. A failure signature can be seen as a set of symptoms associated with a particular defect. These symptoms are directly related to the extraction of specific vibration signals characteristics, which may have stationary, non-stationary, and non-linear peculiarities.

Table 2 Ranges of severity

Vibration speed RMS	States
$V_{\mathrm{RMS}} < 1.15 V_r^{(\mathrm{dir})}$	Excellent
$1.15 V_r^{(\mathrm{dir})} \leqslant V_{\mathrm{RMS}} < V_r^{(\mathrm{dir})}$	Good
$1.25 V_r^{(\mathrm{dir})} \leqslant V_{\mathrm{RMS}} < 1.35 V_r^{(\mathrm{dir})}$	Regular
$V_{\mathrm{RMS}} \geqslant 1.35 V_r^{(\mathrm{dir})}$	Critical

Using the raw data vibration signals would result in three input vectors, one for each direction, with 150,000 elements each. This is a result of a 50-kHz sampling rate alongside a data collection time of 3 s. As a consequence, the following features were extracted from each acceleration signal to decrease the amount of information used by the classifiers, namely crest factor, skewness, motor speed, and the three peaks of the signal frequency spectrum obtained from the Fourier fast transform algorithm. Such features are described in the following.

Crest factor is the ratio between peak value (a_{P}) and the RMS value of the signal (a_{RMS}):

$$F_C = \frac{a_{\mathrm{P}}}{a_{\mathrm{RMS}}}, \tag{2}$$

which should be computed for each of the three directions (X, Y, Z).

Skewness is the third central moment in a distribution. It can be understood as a measure of the asymmetry of the probability distribution of a real data in relation to its average [53]. The skewness of a random variable X can be obtained from

$$S = \frac{\mathbb{E}\left[(X-\mu)^3\right]}{\mathbb{E}\left[(X-\mu)^2\right]^{3/2}}, \tag{3}$$

where μ is the mean of X and $\mathbb{E}[\cdot]$ denotes the expected value operator.

The Fourier transform is capable of transforming the vibration signals from the accelerometer that are in the time domain to the frequency domain [54]. The fast Fourier transform (FFT) was used in this paper, since it calculates the discrete time Fourier transform (DFT) with greater speed [55]. The short-time Fourier transform divides the signal into a series of frames. Each one of these is the processed by the DFT and the results are grouped together to produce the final result. The DFT of a signal $x(n)$ is given by:

$$X^{(N)}(k) = \sum_{n=0}^{N-1} x(n) e^{\frac{-2j\pi kn}{N}}. \tag{4}$$

The directions (X, Y, Z) of each vibration signal were analyzed to extract the following: (i) peak in motor rotation speed, (ii) second harmonic of the motor rotation speed, and (iii) third harmonic of the engine rotation speed. This resulted in a total of 9 features. Obtaining the rotation speed of the motor can be done by performing the FFT of the signal obtained from the tachometer. Each operating scenario is thus represented by a vector with 16 characteristics. One element referring to motor rotation speed, three for wave crest factors, three for skewness, and nine referring to the frequency spectrum peaks.

3.3.1 Classifiers

Identification of the fault type was performed using a classification algorithm. Three algorithms were tested with the recorded signals, namely (i) support vector machine (SVM) [56], (ii) K-nearest neighbors (K-NN) [57], and (iii) Random Forest [58].

The SVM is one of the most used methods for solving classification problems [56]. This algorithm can be applied to high-dimensional problems in which a non-linear discrimination is required. The method presents good performance for the identification of problems in rotating machines based on vibration analysis [59]. It has been applied effectively in many branches of engineering, such as fault diagnosis and data mining [60]. The algorithm separates the analyzed data by choosing a hyperplane capable of differentiating the data from two distinct classes. The best hyperplane for SVMs is given by the greatest margin between the two classes. The margin is defined as the maximum width of the area containing no data and that is also parallel to the hyperplane [61]. The algorithm has a few disadvantages. Namely, the learning rate is slow for a large amount of training data. Furthermore, SVMs were initially developed for binary classification, which requires exogenous adaptations for multi-class problems [60].

The K-NN classifier presents high efficiency in motor fault classification problems from vibration signals [56]. The method is supervised and performs a feature-based comparison of database instances. The algorithm works as follows. An instance is described as a point in an n-dimensional feature space. The K instances that are the closest to an example are counted. Finally, the classification is given based on the most frequent class of these neighbors.

Random forest is an ensemble classification technique, which combines a set of decision tree classifiers through a voting process to classify an unknown example. The method is formed of a set of structured tree classifiers where the trees are independent equally divided random vectors. Each tree results in a unit vote for the most popular class for a given input vector. An ensemble classifier is usually more effective than any of the individuals that form it. Decision trees can be considered as unstable classifiers. Unstable classifiers are those where small changes in the training set cause significant changes in the classifier output [58]. The Bagging method is used to minimize this effect, where multiple classifiers can compensate for the bias of a single classifier [62]. Random forests can be tuned by choosing the number of trees that would be able to maximize the classifier's performance.

3.4 Microcontroller interface

An Arduino HC-05 module was used to perform Bluetooth communication. This module works in master mode and uses the serial port protocol. The protocol version is 2.0 + Enhanced Data Rate (EDR) with a speed of 3 Mbits/s, with a maximum dissipation power of 2.5 mW and a maximum data transmission range of 10 m [63]. The Bluetooth communication transmits information regarding the operating status of the motor. The interface also allows the motor to be switched off and on. However, if the motor has been automatically shut down, due to a critical vibration level, it cannot be started remotely for safety reasons. The "Arduino 1" board was used to interface the computer with the "Arduino 2." The latter is connected to the HC-05 module to enable communication with a mobile phone. "Arduino 2" has a relay attached to it in order to shut down the motor in case the severity reaches a critical state. The connection diagram of this setup is described in Fig. 3. Communication between the microcontrollers was performed using the digital pins of the "Arduino 1," where pins D12, D11, D10, and D9 are digital outputs.

Table 3 describes the set of values the digital ports D12 and D11 and the associated motor states. Motor operating condition is conveyed through ports D10 and D9 and the set of values presented in Table 4. These values are then sent to the developed interface.

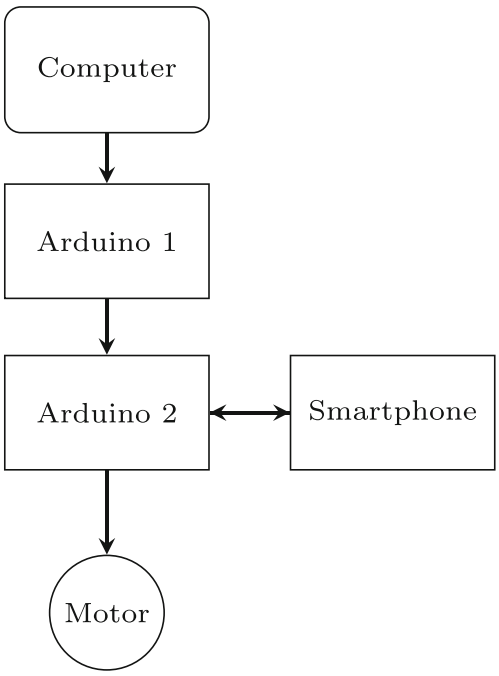

Fig. 3 Diagram of the microcontroller's connection

Table 3 Digital combination for the motor status information

Digital ports		Motor status
D12	D11	
0	0	Excellent
0	1	Good
1	0	Regular
1	1	Critical

3.5 Supervisory system screen

The supervisory system shows the time domain and frequency domain graphs of the acceleration and velocity signals corresponding to the vibration of the three directions, which are axial (X), tangential (Y), and radial (Z). The display also shows the level of vibration severity, the direction with the highest vibration severity level, the motor running state, and the type of defect.

4 Results and discussions

This section presents and discusses the results obtained regarding (i) accelerometer comparison, (ii) motor vibration severity profile, and (iii) classification results. Some of the analyses presented elucidate existing frequency-domain relations that can be valuable for the supervisor system.

4.1 Accelerometer measurement comparison

This section intends to compare the piezoelectric and capacitive accelerometers, in order to choose the most adequate one. Vibration velocity measurements were obtained by integrating the acceleration signal in the frequency domain. Motor rotation was varied in the range $f \in [16, 60]$ (in Hz) with a 2-Hz step under normal motor operating condition (i.e., no faults in the system). This

Table 4 Digital combination for the motor operating condition information

Digital ports		Operating condition
D10	D9	
0	0	Normal
0	1	Imbalance
1	0	Imbalance + Horizontal Misalignment
1	1	Imbalance + Vertical Misalignment

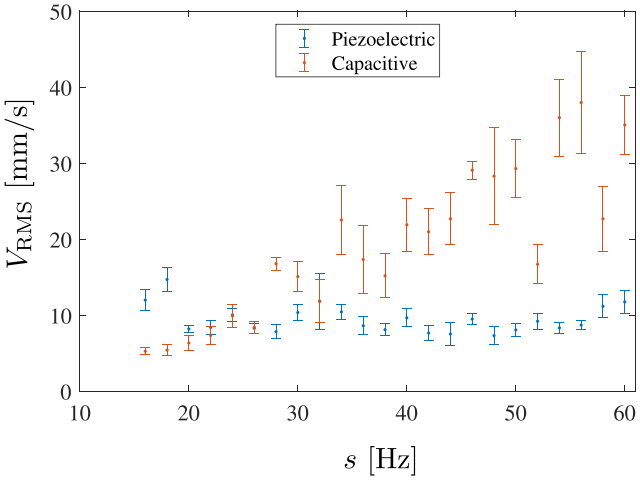

Fig. 4 Comparison of measurements in the X direction

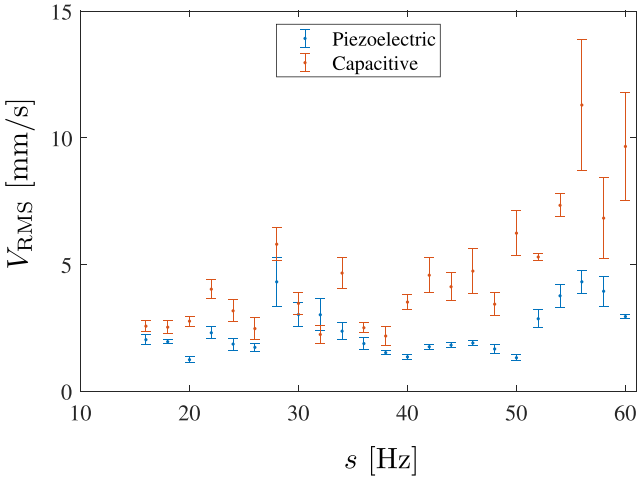

Fig. 6 Comparison of measurements in the Z direction

procedure was repeated five times for each accelerometer, allowing for the verification of sensor repeatability. This was followed by a calculation of the vibration speed RMS values V_{RMS} as a function of (i) the rotor speed s and (ii) the error over the average of the five measurements for each of the motor speeds. This analysis was performed for X, Y, and Z directions, as shown respectively in Figs. 4, 5, and 6, where error bars represent one standard error around the mean. The standard error is defined by

$$E_p \triangleq \frac{\sigma}{\sqrt{n}}, \tag{5}$$

where σ is the standard deviation and $n = 5$ denotes the number of measurements for each rotation speed. Based on the aforementioned plots, the piezoelectric accelerometer presented better repeatability and precision, and was thus the natural choice to be used in the supervisory system.

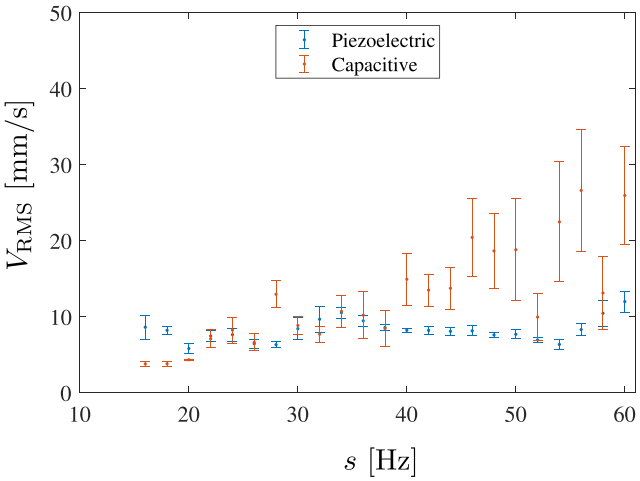

Fig. 5 Comparison of measurements in Y direction

4.2 Motor severity profile survey

Obtaining the severity profile of the machinery being analyzed was performed through three experiments, namely (i) imbalance profiling, (ii) imbalance associated with horizontal misalignment profiling, and (iii) imbalance associated with vertical misalignment profiling. The following sections describe the overall process.

4.2.1 Imbalance severity profiling

An experiment was done for imbalance profiling, in which two different masses were used (6 g and 20 g). For the 6 g mass, rotor speed was set in the range $f \in [16, 60]$ (in Hz) while for 20 g, the speed was set in the range $f \in [16, 50]$ (Hz), the upper range of which was due to a limitation of the simulation bench. Both scenarios considered regular motor operation.

Figure 7 presents V_{RMS} for different configurations along the X direction, namely (i) without an imbalance mass,

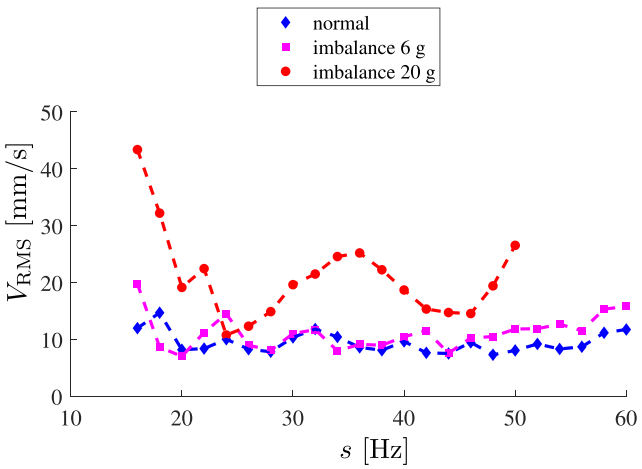

Fig. 7 Imbalance in the X direction

(ii) with a 6 g imbalance mass, and (iii) with a 20 g imbalance mass. Notice that V_{RMS} values for the first two configurations (respectively, normal and 6 g) are similar up to $s = 50$ Hz. The 20 g scenario presents a higher severity analysis than the normal one for low motor speeds (i.e., 16 Hz and 18 Hz). The severity value then drops and rises again as the system enters the resonance region of the X direction, which lies in the interval $f \in [28, 40]$ (Hz). After leaving the resonance region, the severity value starts increasing at approximately 44 Hz.

Figure 8 presents the V_{RMS} data points for the Y direction. The plot shows that the V_{RMS} values for the 6 g mass imbalance scenario approximate the standard operating scenario for low motor speed values (i.e., $f \in [16, 24]$ - in Hz). The vibration RMS values present an increased amplitude due to the system resonance region $f \in [26, 32]$ (Hz). The severity value decreases and rises again starting at 42 Hz. On the other hand, the 20 g mass imbalance scenario for speeds between 16 and 18 Hz has a much higher severity value than the normal one. Note that V_{RMS} value falls and rises again as the system enters the resonance region of the Y direction, which occurs in the $f \in [26, 32]$ (Hz) region. V_{RMS} then increases in rotor speed range $f \in [32, 40]$ Hz and is followed by a reduction in severity, which only increases again at the 50-Hz limit speed.

Figure 9 presents V_{RMS} values for the Z direction. Notice how, for low motor speed values $f \in [16, 20]$ Hz, there is significant overlap between the normal operating scenario and the 6 g imbalance configuration. The V_{RMS} value also exhibits an increased amplitude due to the resonance region of the Z direction system at $f \in [26, 32]$ Hz. The V_{RMS} amplitude value then decreases, rising again from 42 Hz. For low motor speeds $f \in [16, 18]$ Hz, the 20 g mass imbalance scenario alongside the Z direction does not present high severity values, when compared to the normal scenario. This contrasts with the X and Y directions. The resonance region for this direction is in the motor speed range of $f \in [26, 32]$ Hz. After leaving the resonance region, the V_{RMS} value increases in the range $f \in [38, 46]$ (Hz).

The plots presented in this section also show that as the imbalance mass increases so too does the failure severity level. In addition, high vibration severity values do not occur only at high rotation speeds but also in some low frequency rotation values of the motor and also in the probable resonance regions of the system.

4.2.2 Horizontal misalignment imbalance

One possible strategy for assessing horizontal misalignment imbalance can be done by inserting *combined* faults into the system, e.g.: the horizontal misalignment of the motor base can be associated with a 1-mm imbalance defect. Figures 10, 11, and 12 (respectively, the X, Y, and Z directions) show V_{RMS} values for (i) normal scenario, (ii) 6 g imbalance associated with 1-mm horizontal misalignment (rotor speed in range $f \in \{16, 60\}$ Hz), and (iii) 20 g imbalance associated with 1-mm horizontal misalignment (rotor speed range $f \in \{16, 50\}$ Hz).

4.2.3 Vertical misalignment imbalance

This section considers the results obtained by inserting imbalance alongside an 1.27-mm vertical misalignment of the motor base. Figures 13, 14, and 15 (respectively, the X, Y, and Z directions) show V_{RMS} values for (i) normal scenario, (ii) 6 g imbalance associated with 1.27-mm vertical misalignment (rotor speed in range $f \in \{16, 60\}$ Hz), and (iii) 20 g imbalance associated with 1.27-mm vertical misalignment (rotor speed range $f \in \{16, 50\}$ Hz).

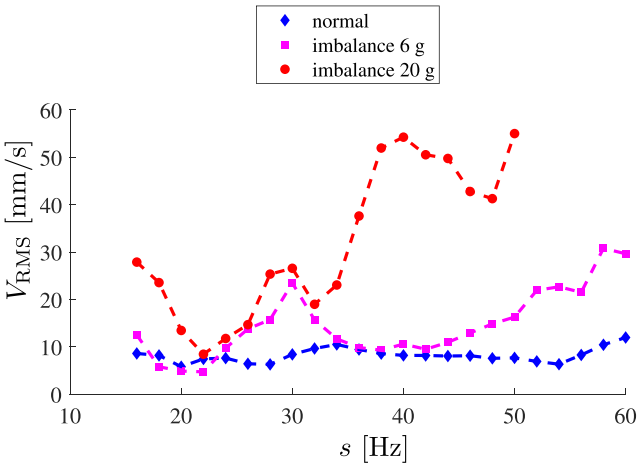

Fig. 8 Imbalance in the Y direction

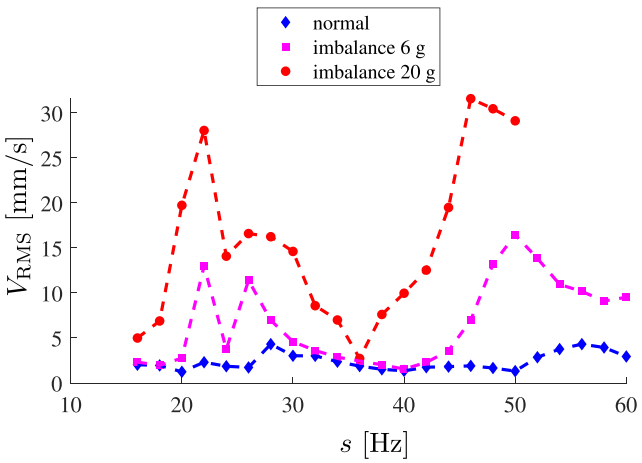

Fig. 9 Imbalance in the Z direction

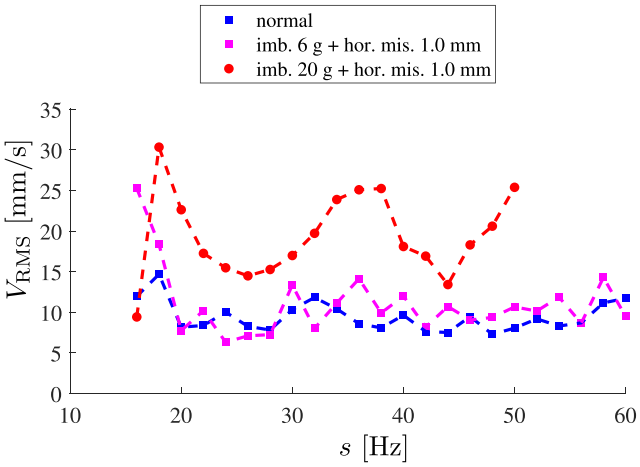

Fig. 10 Horizontal misalignment imbalance in the X direction

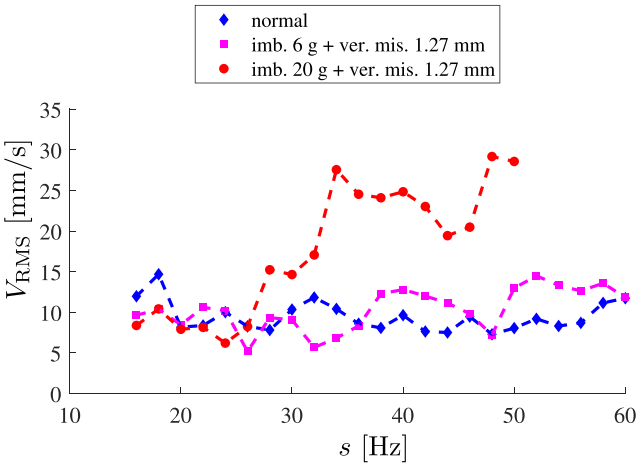

Fig. 13 Vertical misalignment imbalance in the X direction

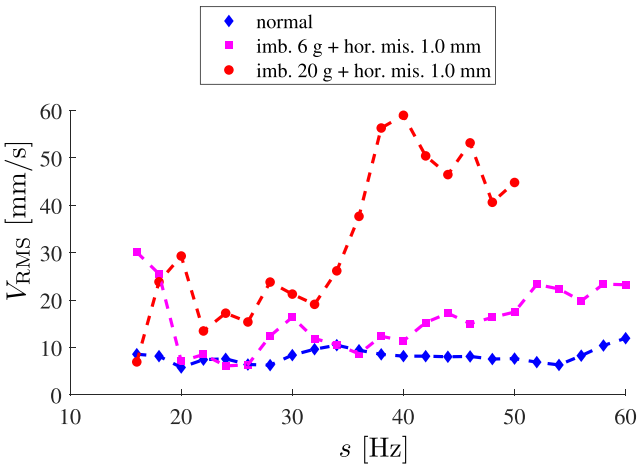

Fig. 11 Horizontal misalignment imbalance in the Y direction

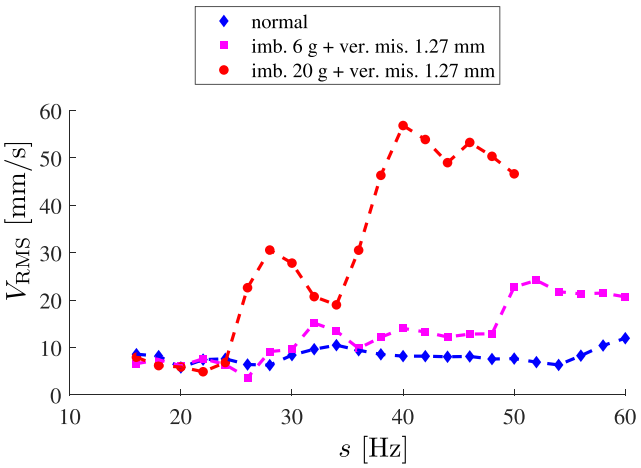

Fig. 14 Vertical misalignment imbalance in the Y direction

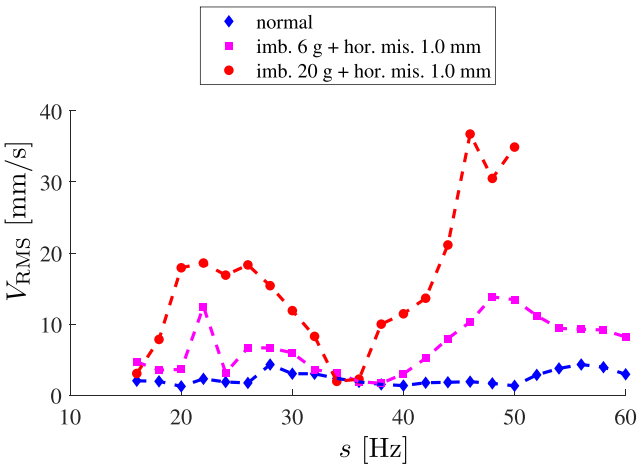

Fig. 12 Horizontal misalignment imbalance in the Z direction

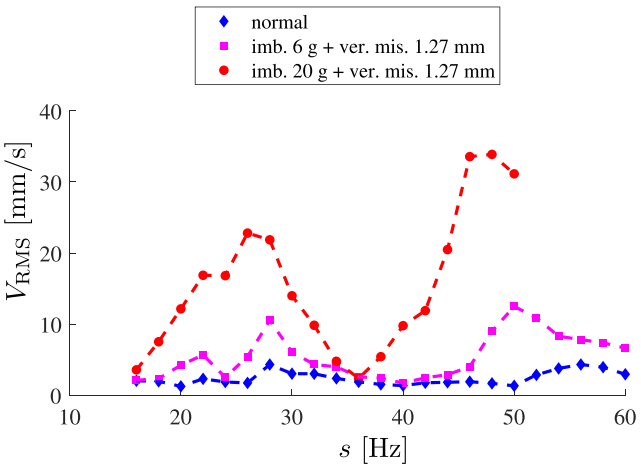

Fig. 15 Vertical misalignment imbalance in the Z direction

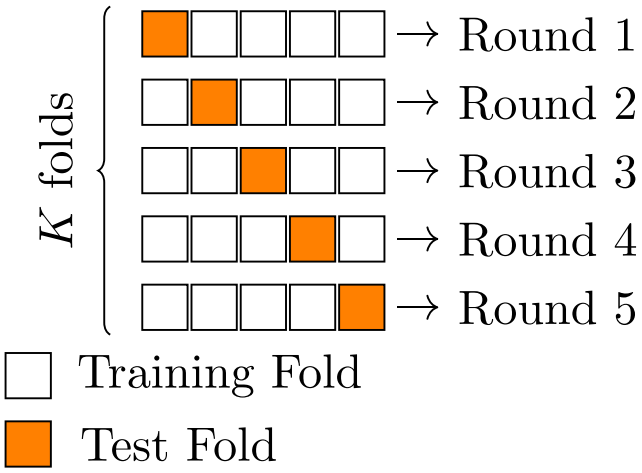

Fig. 16 K-fold representation

The plots presented in Sections 4.2.2 and 4.2.3 show that, in some rotation speeds, the association of misalignment alongside imbalance decreased vibration severity. This was unexpected, since we had assumed that the severity level for two failures would be higher than for a single one. Furthermore, the combination of vertical misalignment and imbalance led to more severe changes than when considering horizontal misalignment with imbalance.

4.3 Classification results

The signals acquired by the piezoelectric accelerometer were divided into 80% for the training phase and 20% for the test phase to measure the classifier's effectiveness, using the K-fold cross-validation method [64]. Five folds were employed, four of these were used for the training set, and one was used for testing purposes. According to [65, 66], this partition is the most suitable when the whole dataset is small. This method selects in each round a test fold representing 20% of the data, while the remaining 4 folds (80%) are employed for training. The method systematically iterates over all possible combinations of test and training folds in order to give an accurate representation of the classification algorithm. This procedure is shown in Fig. 16.

To keep the classes to be identified with a similar number of instances, from a total of 115 normal operating signals, only 41 were chosen to perform the training and testing steps. This effectively enforced class balancing. The evaluation of the three proposed algorithms was based on the confusion matrix, in which the main diagonal corresponds to the correct answers presented by the classifier and the remaining positions to errors. Each term in the matrix is composed of the mean accuracy obtained through the cross-validation process and the respective standard deviation. The classifiers were evaluated through the intraclass average relative accuracy. This metric can be calculated as follows: sum the accuracy values of the main diagonal and divide by the number of classes. This allows for a better represent the overall performance of the classifier when compared to the overall accuracy that can skew the classifier's performance due to the large number of correct answers in a given class [67].

Tables 5, 6, and 7 presents the confusion matrices of testing stages for, respectively, SVM, KNN, and random forests, where:

- C_1 is the normal operating condition;
- C_2 refers to 6g and 20g imbalance;
- C_3 refers to 6g and 20g imbalances associated with 1-mm horizontal misalignment;
- C_4 refers to 6g and 20g imbalances associated with 1.27-mm vertical misalignment.

The hyperparameters of the support vector machine algorithm are the type of kernel function and the regularization term C. An exhaustive search for the optimal hyperparameter values would require a high computational cost. Accordingly, we opted to instead use previously tested values for the regularization term C, namely, $C \in \{2^{-5}, 2^{-3}, 2^{-1}, ...2^{13}, 2^{15}\}$ [68]. As for the gamma parameter, the value obtained was calculated by the autotuning algorithm of MATLAB in order to avoid overfitting. The optimal choice was the one with the highest accuracy value obtained by the intraclass average relative accuracy. The

Table 5 Confusion matrix of the test set using SVM

Output class	Target class (%)			
	C_1	C_2	C_3	C_4
C_1	**94.42 ± 13.73**	13.30 ± 14.84	2.00 ± 4.47	0 ± 0
C_2	5.58 ± 13.73	**42.63 ± 16.18**	32.06 ± 16.51	4.00 ± 9.29
C_3	0 ± 0	22.41 ± 12.19	**57.44 ± 14.95**	6.5 ± 6.02
C_4	0 ± 0	21.66 ± 11.44	8.19 ± 9.52	**89.05 ± 13.96**

The values in bold represent the accuracies of each class (C1,...,C4) for the classifiers SVM, KNN and RF, respectively

Table 6 Confusion matrix of the test set using KNN

Output class	Target class (%)			
	C_1	C_2	C_3	C_4
C_1	**97.92 ± 4.97**	9.30 ± 10.39	2.32 ± 4.97	0 ± 0
C_2	0 ± 0	**65.12 ± 16.37**	20.93 ± 9.21	6.98 ± 10.11
C_3	2.08 ± 4.97	18.60 ± 16.72	**69.77 ± 11.85**	2.32 ± 4.97
C_4	0 ± 0	6.98 ± 6.36	6.98 ± 9.94	**90.70 ± 14.55**

The values in bold represent the accuracies of each class (C1,...,C4) for the classifiers SVM, KNN and RF, respectively

proportion of training samples employed by the SVM in relation to the number of features may also also result in overfitting issues.

The use of the appropriate kernel type will depend on the type of dataset. As there are several types of kernel functions, a bibliographic search was made in order to decrease the amount of functions to be applied in the SVM algorithm. This resulted in the linear kernel, RBF, and Gaussian functions being preselected [69–71]. From these, the linear kernel was the one determined to best suit this work.

The term C comes from cost, it establishes the harmony between training errors and classification margins in order to allow flexibility in class distinction. Term C thus regulates the complexity of the classifier model in relation to the classifier errors in the training stage [72]. For each type of kernel function, different values of $C \in \{2^{-5}, 2^{-3}, 2^{-1}, ...2^{13}, 2^{15}\}$ were tested [68]. The best model for this algorithm was the one that uses the polynomial grade 1 kernel function with $C = 2048$. The optimum choice of hyperparamaters was made by the highest value obtained by the average intraclass relative accuracy of SVM.

The result obtained using the SVM algorithm are shown in Table 5. This algorithm reached an accuracy of 70.88% associated with a standard deviation of 6.37% after tuning some of the hyperparameters present in the model.

K-NN performance classification is presented in Table 6. The algorithm achieved an accuracy of 80.88% associated with a standard deviation of 6.74%. This was achieved using $k = 1$ (i.e., only the nearest neighbor was taken into account for classification purposes) and employing the normalized euclidean distance.

The random forest was the one with the best results. Thus, it was used to compose the supervisory system. Calculating the mean of the main diagonal values of the confusion matrix, we obtained an accuracy of 81.41% associated with a standard deviation of 6.92%, using 76 trees. The division rule used to form the nodes of the trees of random forest was the Gini diversity criterion. The minimum number of observations per leaf used by the classifier was 5. The number of features randomly selected at each node was 4.

The confusion matrix of the random forest classifier (see Table 7) shows a low rate of false positives, that is, scenarios that have defects (C_2, C_3, C_4) but have been classified as normal scenarios (C_1) [73]. A large number of false positives are harmful to this application since failing to identify a defective failure can cause catastrophic damage to the equipment, generating financial losses and exposing workers to the risk of accidents. Table 7 also shows a low rate of false negatives, that is, scenarios that are of normal operation, but were classified as a defective class [73]. A high number of false positives is inconvenient, as it causes unnecessary maintenance stops as in these cases the machine is functioning properly, causing production losses due to unnecessary machine downtime.

Table 7 Confusion matrix of the test set using random forest

Output class	Target class (%)			
	C_1	C_2	C_3	C_4
C_1	**91.78 ± 8.45**	2.22 ± 4.97	0	2.22 ± 4.97
C_2	2.00 ± 4.47	**72.50 ± 18.17**	11.67 ± 13.63	8.89 ± 14.49
C_3	6.22 ± 5.70	13.33 ± 14.49	**81.39 ± 10.09**	8.89 ± 9.29
C_4	0 ± 0	11.95 ± 8.87	6.94 ± 6.36	**80.00 ± 22.70**

The values in bold represent the accuracies of each class (C1,...,C4) for the classifiers SVM, KNN and RF, respectively

5 Conclusions

Properly identifying failure profile severity is key for maintaining the operating status of machinery. This allows for maintenance to be performed before machine failure. Most works focusing on fault classification in rotating machines are concerned with simple faults. This research presented an effective methodology for classification and severity measurement. Unfortunately, to the authors knowledge, there are no previous studies addressing the combined failures of imbalance and misalignment to compare our results with. In addition to the greater part of the work on fault classification in rotating machines, the previous papers on this area are mainly concerned with the development of pre-processing techniques, feature extraction, or performing defect classification.

In this paper, the system is capable of using artificial intelligence algorithms in conjunction with a supervisory system to monitor the state of a rotating machine and controls its operation when necessary. This paper focused on the possibility of differentiating the types of combined faults using intelligent algorithms. An accuracy of 81.41% using a random forest classifier was achieved. The experiments showed that the piezoelectric accelerometer had a better performance than the capacitive one. The frequency-domain integration method demonstrated to be effective for severity measuring applications in rotating machines. Severity failure profiles for different scenarios were constructed, namely, normal operating conditions, imbalance failure, imbalance failure with horizontal misalignment, and imbalance failure with vertical misalignment. One may conclude that high vibration severity values occur in some low motor speed frequency ranges, namely, those in the system resonance regions. Severe vibration was also observed at high speeds. For some cases which combined misalignment with imbalance the vibration severity decreased, which was unexpected. When studying vertical misalignment alongside imbalance, we were able to observe that this resulted in more changes to the severity profile than those resulting from horizontal misalignment and imbalance.

For future work, techniques for reducing the feature space such as PCA (principal component analysis), autoencoder, and KDA (kernel discriminant analysis) will also be evaluated in order to seek to improve classifier performance. We intend to investigate the influence of class imbalance in classifier accuracy that results from data augmentation techniques. Furthermore, we intend to perform simulations that extend the classes originally employed with isolated problems of vertical misalignment, horizontal misalignment, and combined faults composed of horizontal and vertical misalignment.

Author contribution Experimentation: Dionísio Martins, Denys Viana, Ricardo Gutiérrez, and Ulisses Monteiro. Original draft writing: Dionísio Martins, Milena Pinto, and Luís Tarrataca. Review and editing: Amaro Lima, Thiago Prego, Fabrício Lopes e Silva, and Diego Haddad.

Funding This research was supported in part by Brazilian Federal Agencies: CEFET-RJ, CAPES, CNPq, and FAPERJ.

Data availability The dataset generated in this paper is available from the corresponding author on reasonable request.

Code availability The custom software code generated during the current study is not publicly available due to confidentiality policy.

Declarations

Competing interests The authors declare that they have no conflict of interest.

References

1. Rafael LD, Jaione GE, Cristina L, Ibon SL (2020) An industry 4.0 maturity model for machine tool companies. Technol Forecast Soc Change 159:120203
2. Qian W, Li S, Jiang X (2019) Deep transfer network for rotating machine fault analysis. Pattern Recognit 96:106993
3. Li P, Hu W, Hu R, Chen Z (2020) Imbalance fault detection based on the integrated analysis strategy for variable-speed wind turbines. Int J Elect Power Energ Syst 116:105570
4. Yu K, Lin TR, Ma H, Li H, Zeng J (2019) A combined polynomial chirplet transform and synchroextracting technique for analyzing nonstationary signals of rotating machinery. IEEE Trans Instrum Meas 69(4):1505–1518
5. Ma H, Zeng J, Feng R, Pang X, Wang Q, Wen B (2015) Review on dynamics of cracked gear systems. Eng Fail Anal 55:224–245
6. Djagarov N, Grozdev Z, Enchev G, Djagarov J (2019) Ship's induction motors fault diagnosis. In: 2019 16th conference on electrical machines, drives and power systems. IEEE, ELMA, pp 1–4
7. Goyal D, Pabla B, Dhami S et al (2019) Non-contact sensor placement strategy for condition monitoring of rotating machine-elements. Eng Sci Technol Int J 22(2):489–501
8. Li X, Zhang W, Ding Q, Li X (2020) Diagnosing rotating machines with weakly supervised data using deep transfer learning. IEEE Trans Indust Inform 16(3):1688–1697
9. Wang J, Du G, Zhu Z, Shen C, He Q (2020) Fault diagnosis of rotating machines based on the emd manifold. Mechan Syst Signal Process 135:106443
10. Li X, Yang X, Yang Y, Bennett I, Mba D (2019) A novel diagnostic and prognostic framework for incipient fault detection and remaining service life prediction with application to industrial rotating machines. Appl Soft Comput 82:105564
11. Cerrada M, Sánchez R-V, Li C, Pacheco F, Cabrera D, de Oliveira JV, Vásquez RE (2018) A review on data-driven fault severity assessment in rolling bearings. Mech Syst Signal Process 99:169–196
12. Cui L, Jin Z, Huang J, Wang H (2019) Fault severity classification and size estimation for ball bearings based on vibration mechanism. IEEE Access 7:56107–56116

13. Zidat F, Lecointe J-P, Morganti F, Brudny J-F, Jacq T, Streiff F (2010) Non invasive sensors for monitoring the efficiency of ac electrical rotating machines. Sensors 10(8):7874–7895
14. Glowacz A (2018) Acoustic based fault diagnosis of three-phase induction motor. Appl Acoust 137:82–89
15. Teng W, Ding X, Cheng H, Han C, Liu Y, Mu H (2019) Compound faults diagnosis and analysis for a wind turbine gearbox via a novel vibration model and empirical wavelet transform. Renewable Energ 136:393–402
16. Yang F, Habibullah MS, Zhang T, Xu Z, Lim P, Nadarajan S (2016) Health index-based prognostics for remaining useful life predictions in electrical machines. IEEE Trans Ind Electron 63(4):2633–2644
17. Singleton RK, Strangas EG, Aviyente S (2016) The use of bearing currents and vibrations in lifetime estimation of bearings. IEEE Trans Ind Inform 13(3):1301–1309
18. Ahmad W, Khan SA, Kim J-M (2017) A hybrid prognostics technique for rolling element bearings using adaptive predictive models. IEEE Trans Ind Electron 65(2):1577–1584
19. Yan M, Wang X, Wang B, Chang M, Muhammad I (2020) Bearing remaining useful life prediction using support vector machine and hybrid degradation tracking model. ISA Trans 98:471–482
20. Xia M, Li T, Shu T, Wan J, De Silva CW, Wang Z (2018) A two-stage approach for the remaining useful life prediction of bearings using deep neural networks. IEEE Trans Ind Inform 15(6):3703–3711
21. Chen Y, Peng G, Zhu Z, Li S (2020) A novel deep learning method based on attention mechanism for bearing remaining useful life prediction. Appl Soft Comput 86:105919
22. Glowacz A, Glowacz W (2018) Vibration-based fault diagnosis of commutator motor. Shock Vib 2018:1–10
23. Scheffer C, Girdhar P (2004) Practical machinery vibration analysis and predictive maintenance. Elsevier, Amsterdam
24. Lees AW (2016) Vibration problems in machines: Diagnosis and resolution. CRC Press, Boca Raton
25. Mitra S, Koley C (2016) An automated scada based system for identification of induction motor bearing fault used in process control operation. In: 2016 2nd international conference on control, instrumentation, energy & communication (CIEC). IEEE, New York, pp 294-298
26. Hujare DP, Karnik MG (2018) Vibration responses of parallel misalignment in al shaft rotor bearing system with rigid coupling. Mater Today Proc 5(11):23863–23871
27. Bai C, Ganeriwala SS, Sawalhi N (2019) A rational basis for determining vibration signature of shaft/coupling misalignment in rotating machinery. In: Rotating Machinery, Vibro-Acoustics & Laser Vibrometry, vol 7. Springer, pp 207–217
28. Peeters C, Leclère Q, Antoni J, Lindahl P, Donnal J, Leeb S, Helsen J (2019) Review and comparison of tacholess instantaneous speed estimation methods on experimental vibration data. Mech Syst Signal Process 129:407–436
29. International Organization for Standardization (2016) I. 21940-11:2016, Mechanical vibration – rotor balancing– part 11: Procedures and tolerances for rotors with rigid behaviour, ISO 21940-11
30. Yamamoto GK, da Costa C, da Silva Sousa JS (2016) A smart experimental setup for vibration measurement and imbalance fault detection in rotating machinery. Case Stud Mechan Syst Signal Process 4:8–18
31. Klausen A, Van Khang H, Robbersmyr KG (2018) Novel threshold calculations for remaining useful lifetime estimation of rolling element bearings. In: 2018 XIII International Conference on Electrical Machines (ICEM). IEEE, New York, pp 1912-1918
32. Sharma A, Amarnath M, Kankar P (2016) Feature extraction and fault severity classification in ball bearings. J Vib Control 22(1):176–192
33. Chang H-C, Jheng Y-M, Kuo C-C, Hsueh Y-M (2019) Induction motors condition monitoring system with fault diagnosis using a hybrid approach. Energies 12(8):1471
34. Umbrajkaar A, Krishnamoorthy A, Dhumale R (2020) Vibration analysis of shaft misalignment using machine learning approach under variable load conditions. Shock and Vibration
35. Lu S, He Q, Wang J (2019) A review of stochastic resonance in rotating machine fault detection. Mech Syst Signal Process 116:230–260
36. William PE, Hoffman MW (2011) Identification of bearing faults using time domain zero-crossings. Mechan Syst Signal Process 25(8):3078–3088
37. Zhang A, Hu F, He Q, Shen C, Liu F, Fanrang K (2014) Doppler shift removal based on instantaneous frequency estimation for wayside fault diagnosis of train bearings. J Vibrat Acoust 136:021019
38. Yu G (2019) A concentrated time–frequency analysis tool for bearing fault diagnosis. IEEE Trans Instrum Meas 69(2):371–381
39. Wang H, Li S, Song L, Cui L (2019) A novel convolutional neural network based fault recognition method via image fusion of multi-vibration-signals. Comput Ind 105:182–190
40. Sugumaran V, Muralidharan V, Ramachandran K (2007) Feature selection using decision tree and classification through proximal support vector machine for fault diagnostics of roller bearing. Mechan Syst Signal Process 21(2):930–942
41. Lin C-J, Chu W-L, Wang C-C, Chen C-K, Chen I-T (2019) Diagnosis of ball-bearing faults using support vector machine based on the artificial fish-swarm algorithm. J Low Frequency Noise Vibrat Act Cont 1–14
42. Zhang L, Xiong G, Liu H, Zou H, Guo W (2010) Bearing fault diagnosis using multi-scale entropy and adaptive neuro-fuzzy inference. Expert Syst Appl 37(8):6077–6085
43. Wang N, Jiang D (2018) Vibration response characteristics of a dual-rotor with unbalance-misalignment coupling faults: Theoretical analysis and experimental study. Mech Mach Theory 125:207–219
44. Srinivas RS, Tiwari R, Kannababu C (2019) Model based analysis and identification of multiple fault parameters in coupled rotor systems with offset discs in the presence of angular misalignment and integrated with an active magnetic bearing. J Sound Vib 450:109–140
45. Dekhane A, Djellal A, Boutebbakh F, Lakel R (2020) Cooling fan combined fault vibration analysis using convolutional neural network classifier. In: Proceedings of the 3rd international conference on networking, information systems & security, pp 1–6
46. Ghemari Z, Salah S, Bourenane R (2018) Resonance effect decrease and accuracy increase of piezoelectric accelerometer measurement by appropriate choice of frequency range. Shock Vib 2018:1–8
47. Mohammed Z, Elfadel IAM, Rasras M (2018) Monolithic multi degree of freedom (mdof) capacitive mems accelerometers. Micromachines 9(11):602
48. Fraden J (2010) Handbook of modern sensors, vol 3. Springer, New York
49. Shiroishi J, Li Y, Liang S, Kurfess T, Danyluk SE, Walczak B, Massart D (2016) International standard organization-iso 10816-1, Mechanical vibration–evaluation of machine vibration by measurements on non-rotating part 1
50. Zhu Y, Jiang W, Kong X, Zheng Z, Hu H (2015) An accurate integral method for vibration signal based on feature information extraction. Shock Vib 2015:1–13
51. Han S (2010) Measuring displacement signal with an accelerometer. J Mech Sci Technol 24(6):1329–1335

52. Qihe L (2019) Integration of vibration acceleration signal based on labview. In: Journal of physics: conference series, vol 1345. IOP Publishing, p 042067
53. Cocconcelli M, Curcurú G, Rubini R (2017) Statistical evidence of central moment as fault indicators in ball bearing diagnostics. In: The international conference surveillance 9, MAR, pp 1–10
54. Haykin SS, Van Veen B (2001) Sinais e sistemas. Bookman, South Carolina
55. Sikder N, Bhakta K, Al Nahid A, Islam MM (2019) Fault diagnosis of motor bearing using ensemble learning algorithm with fft-based preprocessing. In: 2019 international conference on robotics, electrical and signal processing techniques (ICREST). IEEE, New York, pp 564-569
56. Liu R, Yang B, Zio E, Chen X (2018) Artificial intelligence for fault diagnosis of rotating machinery: A review. Mech Syst Signal Process 108:33–47
57. Wang P, Tamilselvan P, Hu C (2014) Health diagnostics using multi-attribute classification fusion. Eng Appl Artif Intell 32:192–202
58. Breiman L (2001) Random forests. Machin Learn 45(1):5–32
59. Xu J, Xu C, Zou B, Tang YY, Peng J, You X (2018) New incremental learning algorithm with support vector machines. IEEE Trans Syst Man Cybern Syst 49(11):2230–2241
60. Zheng J, Pan H, Cheng J (2017) Rolling bearing fault detection and diagnosis based on composite multiscale fuzzy entropy and ensemble support vector machines. Mech Syst Signal Process 85:746–759
61. Malla C, Rai A, Kaul V, Panigrahi I (2019) Rolling element bearing fault detection based on the complex morlet wavelet transform and performance evaluation using artificial neural network and support vector machine. Noise Vibrat Worldw 50(9-11):313–327
62. Acuna E, Rojas A (2001) Bagging classifiers based on kernel density estimators. In: Proceedings of the international conference on new trends in computational statistics with biomedical applications, pp 343–350
63. I. Studio Hc-05-bluetooth to serial port module, Datasheet, June (2010)
64. Wong T, Yang N (2017) Dependency analysis of accuracy estimates in k-fold cross validation. IEEE Trans Knowl Data Eng 29(11):2417–2427
65. Rodriguez JD, Perez A, Lozano JA (2009) Sensitivity analysis of k-fold cross validation in prediction error estimation. IEEE Trans Pattern Anal Machin Intell 32(3):569–575
66. Ljumović M, Klar M (2015) Estimating expected error rates of random forest classifiers: a comparison of cross-validation and bootstrap. In: 2015 4th mediterranean conference on embedded computing (MECO). IEEE, New York, pp 212-215
67. MARTINS DH et al (2017) Predictive maintenance based on mechanical unbalance severity analysis of rotating machines. In: 24Th ABCM international congress of mechanical engineering. ABCM
68. Jin Y, Huang J, Zhang J et al (2011) Study on influences of model parameters on the performance of svm. In: 2011 International conference on electrical and control engineering. IEEE, pp 3667–3670
69. Elangovan M, Sugumaran V, Ramachandran K, Ravikumar S (2011) Effect of svm kernel functions on classification of vibration signals of a single point cutting tool. Expert Syst Appl 38(12):15202–15207
70. Kumar A, Kumar R (2017) Time-frequency analysis and support vector machine in automatic detection of defect from vibration signal of centrifugal pump. Measurement 108:119–133
71. Santos P, Villa LF, Reñones A, Bustillo A, Maudes J (2015) An svm-based solution for fault detection in wind turbines. Sensors 15(3):5627–5648
72. Kou D, Zhang Y, Zheng H (2010) A parameters selection method of svm. In: 2010 International conference on computational intelligence and software engineering. IEEE, pp 1–4
73. Neuzil J, Kreibich O, Smid R (2013) A distributed fault detection system based on iwsn for machine condition monitoring. IEEE Trans Ind Inform 10(2):1118–1123